SPE-211095-MS

Rapid NMR T2 Extraction from Micro-CT Images Using Machine Learning

Yiteng Li and Xupeng He, King Abdullah University of Science and Technology; Marwa Alsinan and Hyung Kwak, Saudi Aramco; Hussein Hoteit, King Abdullah University of Science and Technology

 DOI 10.2118/211095-MS

This paper was prepared for presentation at the ADIPEC held in Abu Dhabi, UAE, 31 October – 3 November 2022.

Abstract

Nuclear magnetic resonance (NMR) is an important tool for characterizing pore size distributions of reservoir rocks. Pore-scale simulations from digital rocks (micro-CT images) provide deep insights into the correlation between pore structures and NMR relaxation processes. Conventional NMR simulations using the random walk method could be computationally expensive at high image resolution and particle numbers. This work introduces a novel machine-learning-based approach as an alternative to conventional random walk simulation for rapid estimation of NMR magnetization signals.

This work aims to establish a "value-to-value" model using artificial neural networks to create a nonlinear mapping between the input of Minkowski functionals and surface relaxivity, and NMR magnetization signals as the output. The proposed workflow includes three main steps. The first step is to extract subvolumes from digital rock duplicates and characterize their pore geometry using Minkowski functionals. Then random walk simulations are performed to generate the output of the training dataset. An optimized artificial neural network is created using the Bayesian optimization algorithm.

Numerical results show that the proposed model, with fewer inputs and simpler network architecture than the referenced model, achieves an excellent prediction accuracy of 99.9% even for the testing dataset. Proper data preprocessing significantly improves training efficiency and accuracy. Moreover, the inputs of the proposed model are more pertinent to NMR relaxation than the referenced model that used twenty-one textural features as input. This works offers an accurate and efficient approach for the rapid estimation of NMR magnetization signals.

Introduction

NMR logging is an important technique for measuring the petrophysical properties of reservoir rocks (Coates, 1999). It produces measurable signals in the form of transverse relaxation time (also known as T_2) by inverting NMR magnetization responses (Kwak et al., 2019). Complex reservoir rock structures heavily affect NMR magnetization decay, raising huge challenges in the accurate interpretation of pore size distribution at the field scale. Thus, pore-scale NMR simulations offer deep insights into the relationship between pore structures and NMR relaxation processes (Li et al., 2022).

Typically, there are two classes of simulation methods, namely the mesh-based method and the mesh-free method. The mesh-based method solves Bloch-Torrey equations for NMR magnetization amplitudes such as using the finite element method (Connolly et al., 2019; Ghomeshi et al., 2018; Mohnke & Klitzsch, 2010). It is well known that solving partial differential equations requires a sophisticated solver. Moreover, it is prohibitively expensive to solve an enormous system as a digital rock model usually has millions of grid blocks. As an alternative, many commercial applications and open-source programs use the mesh-free random walk method, because of its easy implementation and parallelism. In this class of methods, particles diffuse in the Brownian motion, and they only travel within the pore space (Benavides et al., 2017; Li et al., 2022; Talabi, 2008). A sufficient number of particles, ranging from tens of thousands to millions is needed, raising a moderate to high computational cost. In addition, the computational efficiency of random walk simulations also depends on the image resolution. With the resolution increasing to 1 um or submicron scale, the simulation will become time-consuming. It is unaffordable to perform a random walk simulation without either CPU parallelism or GPU acceleration.

In recent years, machine learning (ML) techniques have rapidly grown, and they have been extensively applied in the petroleum engineering community. It has been widely demonstrated that ML technology is competitive with traditional simulation methods, provided that a well-designed network is trained with a high-quality data set. There are four classes of neural networks, each of which is designed for particular problems. Artificial neural networks (ANNs) specialize in value-to-value applications, including gas injection optimization (He et al., 2021), mud loss prediction (Albattat et al., 2022), fracture permeability evaluation (He et al., 2021b), etc.; convolutional neural networks (CNNs) fit image-to-value regression problems like model upscaling (He et al., 2020; He et al., 2021; Santoso et al., 2019); generative adversarial networks (GANs) focus on image-to-image translation, including image reconstruction (Li et al., 2022; Mosser et al., 2017), image super-resolution (Wang et al., 2018; da Wang et al., 2020), etc.; long-short term memory (LSTM) networks have been successfully applied for time-series problems, such as history matching (Santoso et al., 2021), CO_2 leakage rate forecast (He et al., 2021a), and oil production prediction (Tadjer et al., 2021).

This work utilizes an ANN to predict NMR magnetization signals from micro-CT images. To the best of our knowledge, there was only one reference that attempted to use ANNs to tackle the same issue (Farzi et al., 2017). In that work, the authors predicted NMR magnetization and T_2 responses from micro-CT images using two separate ANN models. Twenty-one textural features were extracted from eight rock samples (six sand packs and two sandstones) for training. However, these features only identified the textures of 2D thin sections and they didn't fully characterize the 3D geometrical properties of a rock sample. Moreover, six samples were far from enough to train a robust ANN model. Instead, in this study, 775 subsamples are extracted from Berea, Bentheimer, and Doddington sandstones, divided into the training, validation, and testing datasets with a ratio of 0.8, 0.1, and 0.1. The 3D geometrical properties, characterized by Minkowski functionals, combined with surface relaxivity are used as input of the proposed neural network. It is shown that the proposed ANN exhibits excellent prediction accuracy, however, with fewer inputs and hidden neurons than the referenced model. It has to be mentioned that training ANNs for NMR T_2 responses prediction is a very challenging task. Even though Farzi et al. (2017) trained a separate ANN for this purpose, which showed fairly good accuracy, no clear evidence was shown in their work on how they selected their training data (no value provided). Technically, their work is not reproducible. At the end of this work, we will give our explanation of why it is so challenging to regress NMR T_2 curves using simple artificial neural networks.

Random walk simulation

The random walk method is the most commonly-used numerical algorithm in commercial and open-source pore-scale NMR simulators (Benavides et al., 2017; Talabi, 2008). It assumes particles (hydrogen nuclei)

diffuse in the form of the Brownian motion within a voxelized structure segmented from micro-CT images. At the very beginning, all the particles, or say walkers, are randomly placed in the pore space. For each time step, walkers diffuse from their previous positions to new positions on a spherical surface with the radius of $ds = \sqrt{6D_0\Delta t}$, where D_0 is the bulk diffusion coefficient of water and Δt is the time step size. The new position of a walker is given by

$$x(t) = x(t_0) + ds\sin\theta\cos\varphi \tag{1}$$

$$y(t) = y(t_0) + ds\sin\theta\sin\varphi \tag{2}$$

$$z(t) = z(t_0) + ds\cos\theta \tag{3}$$

where $\theta \in [0, \pi]$ and $\varphi \in [0, 2\pi]$ are randomized in their given ranges. If a walker collides with a solid voxel, it will bounce back to its previous position and its magnetization amplitude is penalized by a decreasing factor (1-p) (Benavides et al., 2017),

$$p = \frac{2\rho ds}{3D_0} \tag{4}$$

where ρ is the surface relaxivity. If a walker reaches the image boundary, it is enforced to bounce back to its previous position so that the number of walkers remains constant during simulation. In this study, diffusive relaxation is ignored as it is often minimized in laboratory experiments. The diffusion coefficient is set to 2500 um^2/s and the bulk relaxation time is 3.1 seconds. We use 100000 walkers for the NMR relaxation simulation, and it is terminated when the simulation time exceeds 5 seconds. To make sure the random walkers take sufficient steps before reaching the solid-pore interface, the time step size is controlled by setting the diffusing distance to one-third of the image resolution.

Proposed Machine-Learning Workflow

This section attempts to develop a data-driven, physics featuring surrogate model for rapid estimation of NMR magnetization signals. Different from Farzi et al.'s work (2017), three Minkowski functionals and surface relaxivity are used as input, which characterize the 3D pore geometry and relaxation intensity of a given rock sample. Each step of the proposed workflow will be detailed as follows:

1. **Subsample extraction**: The quantity of the training dataset is critical in developing an accurate and robust ANN model. To obtain sufficient rock samples, we extract subvolumes from Bentheimer, Berea, and Doddington sandstones to demonstrate the proposed ML-based method. Each subvolume size is @56×256×256 with a striding window of 128. This preserves the effect of representative elementary volume, increases the data amount, and reduces the overlapping structures between subsamples. Consequently, 775 rock samples are generated, as illustrated in Figure 1, and they are divided into training, validation, and testing sets with a ratio of 0.8, 0.1, and 0.1.
2. **Geometry characterization**: Minkowski functionals are extensively used to characterize the geometry and morphology of 3D porous structures (Armstrong et al., 2019). For each subsample, we calculate three Minkowski functionals that represent its volume, surface area, and total curvature (Euler characteristic) and normalize them in terms of the bulk volume. The zeroth-order Minkowski functional is the porosity,

$$\overline{\mathrm{MF}_0} = \frac{V_{\mathrm{pore}}}{V} \tag{5}$$

The first-order Minkowski functional is the specific surface area

$$\overline{\mathrm{MF}_1} = \frac{S_{\mathrm{interface}}}{V} \tag{6}$$

which controls the surface relaxation rate. The third-order Minkowski functional is the specific Euler characteristic,

$$\bar{\mathrm{MF}}_3 = \frac{1}{4\pi V}\int \frac{1}{r_1 r_2} dS \tag{7}$$

The integral in Eq. (7) can be approximated by the classical Euler formula (Legland et al., 2007)

$$\chi = V - E + F - O \tag{8}$$

where V, E, F and O are the number of vertices, edges, faces and objects, respectively. The Euler characteristic is indicative of the connectivity of porous structures. A positive value indicates the porous phase has good connectivity, so walkers are likely to diffuse from one pore to another before losing its contribution to magnetization amplitude. This becomes more pronounced when macro-porosity is coupled with micro-porosity and surface relaxivity is low. Such a phenomenon is known as diffusion coupling, which raises a huge challenge in accurate interpretation of pore size distribution. We keep the Euler characteristic as one of the inputs as it roughly indicates pore connectivity, even though the understudy sandstones do not have diffusion coupling issues. Figure 2, Figure 3 and Figure 4 display the distribution of porosity, specific surface area, and Euler characteristic for Bentheimer, Berea and Doddington sandstones.

3. **Surrogate model development**: The proposed model takes three Minkowski functionals and surface relaxivity as input to predict one hundred NMR magnetization signals. As we fix the echo time at which NMR magnetization signals are recorded, these data are included for training. To obtain the best network performance, we use Bayesian optimization to optimize the hyperparameters, such as the number of hidden layers, number of neurons, etc. The resultant neural network has a single layer with five neurons. Figure 5 exhibits a schematic diagram of the optimized neural network. To improve the training efficiency and accuracy, all the inputs and outputs are normalized between 0 and 1.

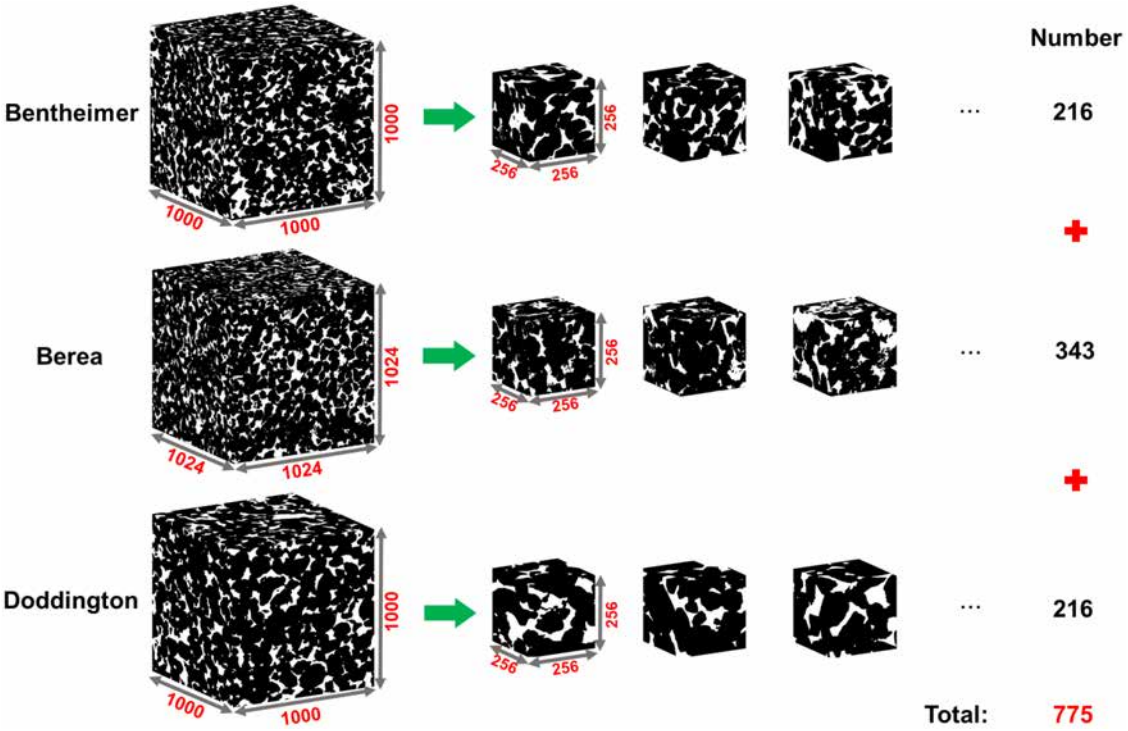

Figure 1—Extracting subvolumes from Bentheimer, Berea, and Doddington sandstones. The subvolume size is 256×256×256, totally 775 subvolumes generated for training.

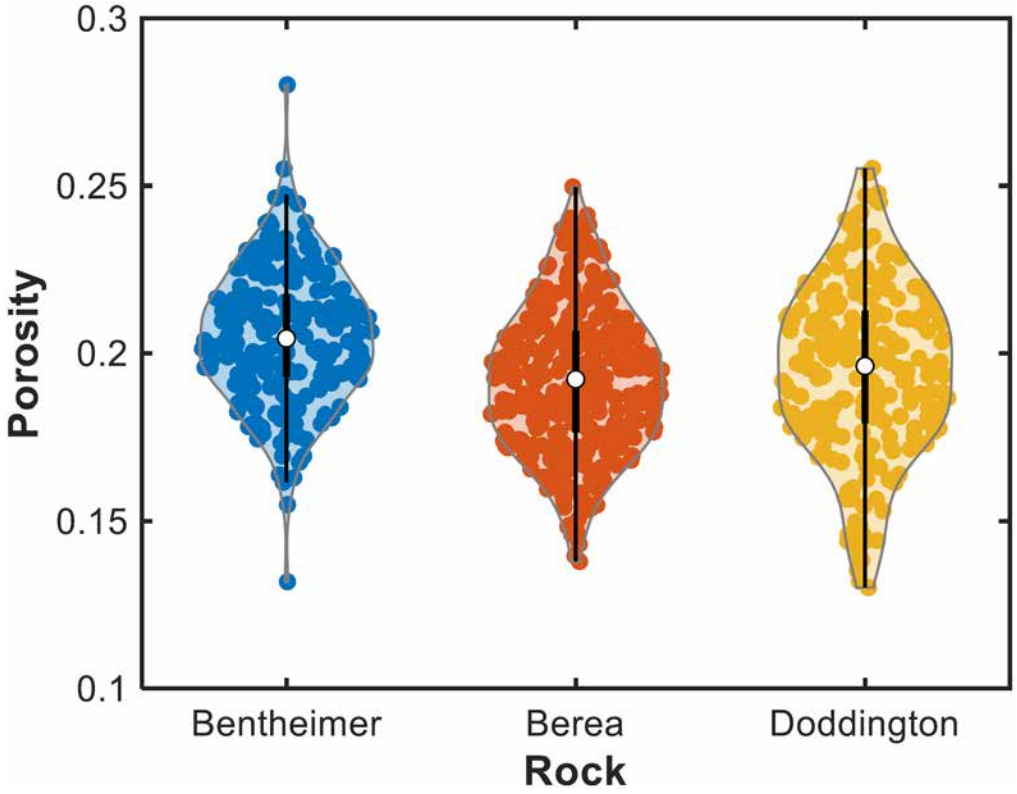

Figure 2—Porosity distribution for Bentheimer, Berea and Doddington sandstones.

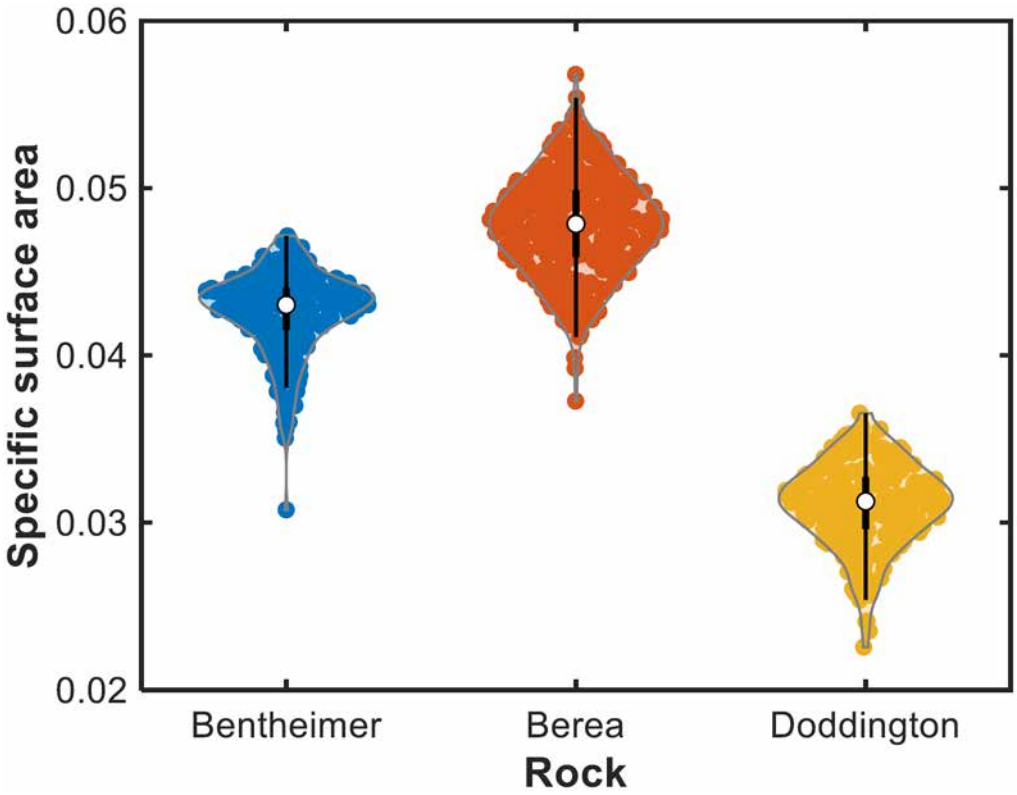

Figure 3—Specific surface area distribution for Bentheimer, Berea and Doddington sandstones.

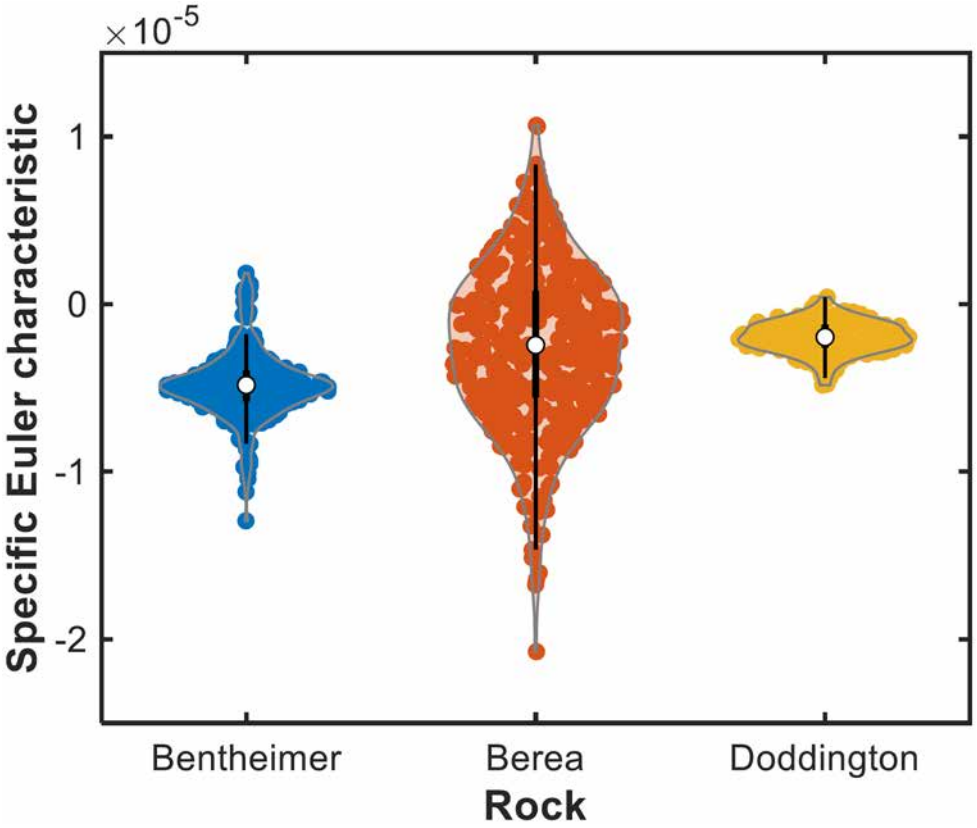

Figure 4—Specific Euler characteristic distribution for Bentheimer, Berea and Doddington sandstones.

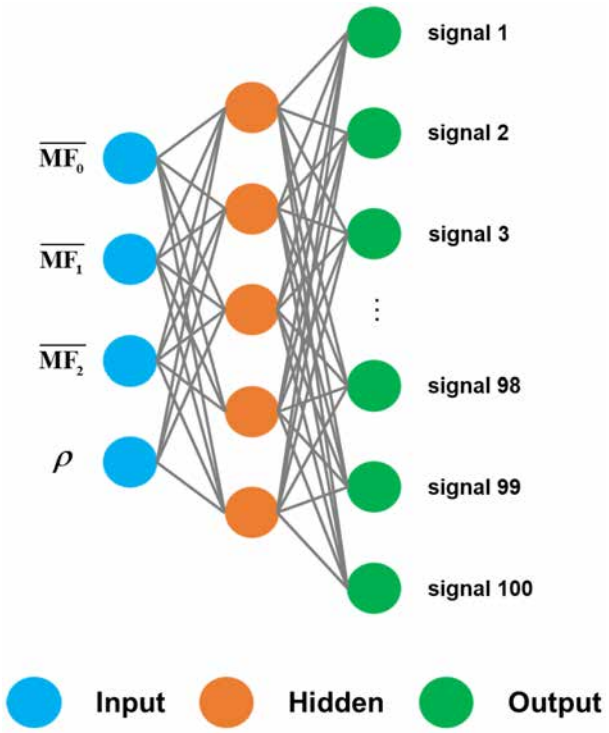

Figure 5—The optimized neural network with a single hidden layer of five neurons.

Results and Discussion

Figure 6 shows the training performance of the proposed ANN model. The mean squared error (MSE) is used as the performance function for training. As seen in Figure 6, MSE declines rapidly in the first five epochs, and then it decays slowly. The best performance is reached at 26 epoch and we don't observe the overfitting issue during training.

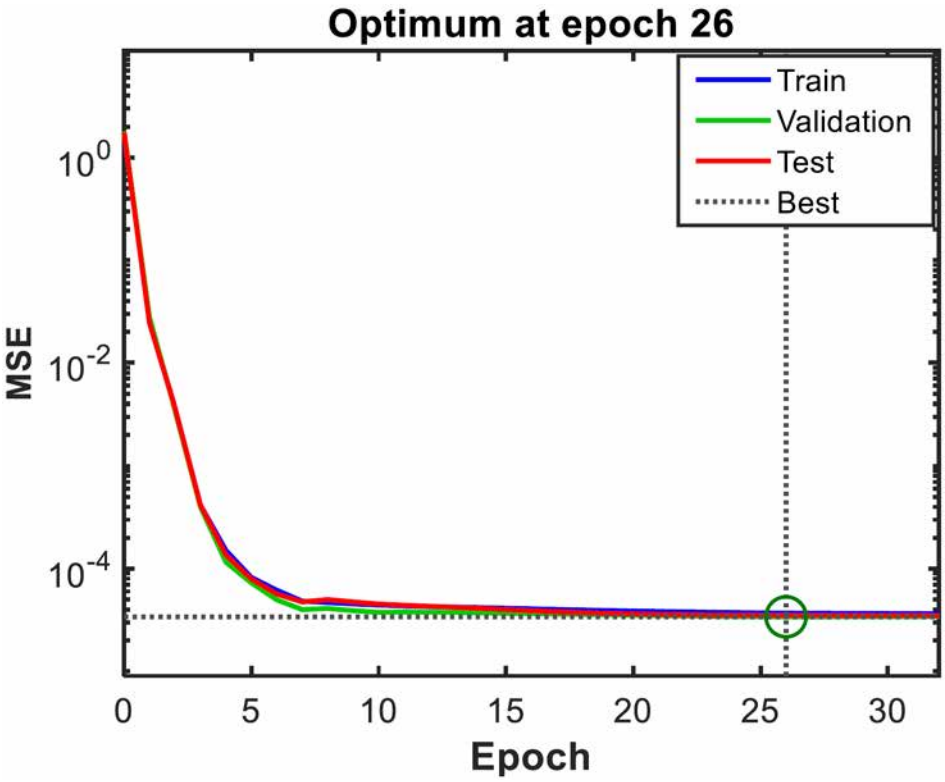

Figure 6—Training performance of the proposed ANN model. The best performance is achieved at 26th epoch.

In Figure 7, the predicted NMR magnetization signals are compared with the ground truth values. Ideally, all the predictions are supposed to align with the diagonal (the black dashed line), meaning that the predicted values are exactly the same as the ground-truth values. In practice, this rarely happens, but still, the proposed ANN achieves excellent prediction accuracy. The root means squared errors (RMSE) for training, validation, and testing data sets are 0.61%, 0.58%, and 0.59%, respectively. The referenced model used 21 textural features as the input and has 14 neurons in a hidden layer. Instead, the proposed model shows a higher prediction accuracy with four input features and five neurons in the hidden layer. Figure 8 illustrates the histogram of errors between the ground truths and predictions. For the given dataset, the visible errors range from -0.03 to 0.03, following a normal distribution. In particular, most errors reside nearby the zero line, with very few at the margin. These features make it practically viable to use the predicted NMR magnetization signals from micro-CT images using the proposed ANN model.

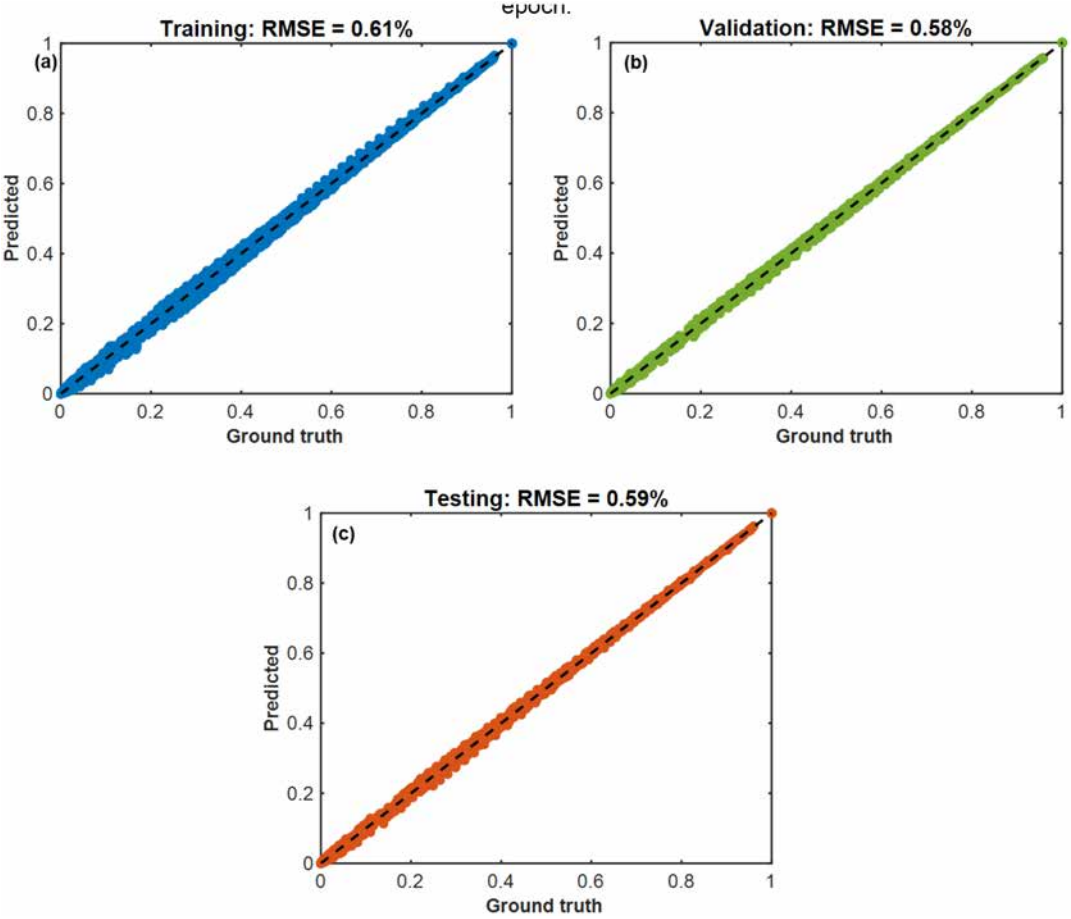

Figure 7—Comparing the predicted NMR magnetization signals with the ground truth for (a) training, (b) validation and (c) testing.

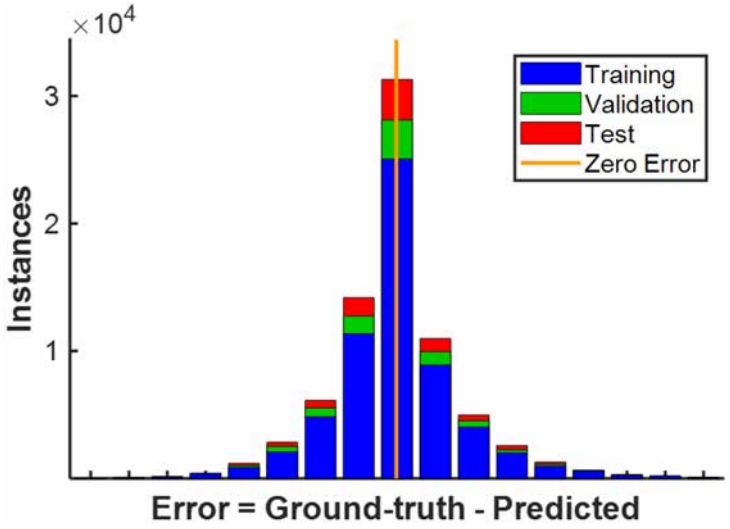

Figure 8—Histogram of prediction errors. Positive values indicate underestimation, while negative values indicate overestimation.

To close this section, it is worth highlighting the difficulty in predicting the NMR T_2 responses using ANNs to interpret reservoir rock properties. Figure 9 shows four T_2 curves of Berea subsamples. The range of T_2 values is truncated between 0.01 to 10 seconds so that T_2 curves stay in the center of the plot. Typically, NMR T_2 responses may range from 0.1 to 10000 seconds. It is not hard to imagine that a T2 curve has

a lot of zero values. The characteristic of unbalanced zero and nonzero values increases the difficulty of regressing NMR T_2 curves. In addition, the multi-modal feature of NMR T_2 curves, especially the sharp uphill and downhill change, raise another challenge in training ANNs to fit NMR T_2 curves. This issue cannot be simply solved by increasing the number of layers and neurons, which in turn increases the risk of overfitting. Therefore, one of our future works is to develop an accurate and robust ML model for rapid estimation of NMR T_2 curves from micro-CT images.

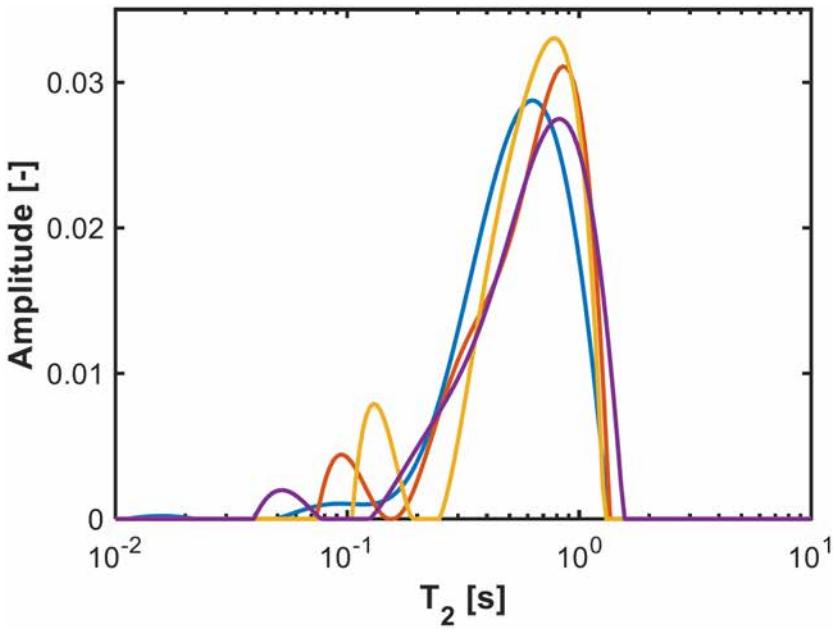

Figure 9—NMR T2 curves for subsamples of Berea sandstones.

Conclusion

In this study, a data-driven ANN model is developed for the rapid estimation of NMR magnetization signals. In contrast to the referenced model, three Minkowski functionals and surface relaxivity are used as the input of the neural network, which characterize the pore geometry and relaxation intensity of rock samples. The proposed method provides an accurate and efficient alternative to the conventional random walk simulation for rapidly estimating NMR magnetization signals from micro-CT images. The main conclusions are summarized below:

- ANN can efficiently and accurately predict NMR magnetization signals.
- A simple network architecture yields very high prediction accuracy with proper data processing.
- Prediction of NMR T_2 responses using artificial neural networks is a challenging task, because of the characteristics of NMR T_2 curves, such as unbalanced zero and nonzero value distributions and multi-modality with sharp peaks.

Future work will be extended to develop a robust deep-learning model to rapidly estimate NMR T_2 responses over a wide range of rock types (including both sandstone and carbonates) and surface relaxivity, as the current ANN model mainly focuses on the sandstones with a few surface relaxivity values.

Acknowledgments

We would like to thank Saudi Aramco for funding this research. We would also like to thank King Abdullah University of Science and Technology (KAUST) for providing a license for MATLAB.

References

Albattat, R., He, X., AlSinan, M., Kwak, H., & Hoteit, H. (2022). Modeling Lost-Circulation in Fractured Media Using Physics-Based Machine Learning. *83rd EAGE Annual Conference & Exhibition*, 2022(1), 1–5.

Armstrong, R. T., McClure, J. E., Robins, V., Liu, Z., Arns, C. H., Schlüter, S., & Berg, S. (2019). Porous media characterization using Minkowski functionals: Theories, applications and future directions. *Transport in Porous Media*, **130**(1), 305–335.

Benavides, F., Leiderman, R., Souza, A., Carneiro, G., & Bagueira, R. (2017). Estimating the surface relaxivity as a function of pore size from NMR T2 distributions and micro-tomographic images. *Computers & Geosciences*, **106**, 200–208.

Coates, G. R. (1999). NMR logging principles and applications. *Halliburton Energy Services*.

Connolly, P. R. J., Yan, W., Zhang, D., Mahmoud, M., Verrall, M., Lebedev, M., Iglauer, S., Metaxas, P. J., May, E. F., & Johns, M. L. (2019). Simulation and experimental measurements of internal magnetic field gradients and NMR transverse relaxation times (T2) in sandstone rocks. *Journal of Petroleum Science and Engineering*, **175**, 985–997.

Farzi, R., Bolandi, V., Kadkhodaie, A., Iglauer, S., & Hashempour, Z. (2017). Simulation of NMR response from micro-CT images using artificial neural networks. *Journal of Natural Gas Science and Engineering*, **39**, 54–61.

Ghomeshi, S., Kryuchkov, S., & Kantzas, A. (2018). An investigation into the effects of pore connectivity on T2 NMR relaxation. *Journal of Magnetic Resonance*, **289**, 79–91.

He, X., Qiao, T., Santoso, R., Hoteit, H., AlSinan, M. M., & Kwak, H. T. (2021). Gas Injection Optimization Under Uncertainty in Subsurface Reservoirs: An Integrated Machine Learning-Assisted Workflow. *ARMA/DGS/SEG 2nd International Geomechanics Symposium*.

He, X., Santoso, R., Alsinan, M., Kwak, H., & Hoteit, H. (2021). Constructing Dual-Porosity Models from High-Resolution Discrete-Fracture Models Using Deep Neural Networks. *SPE Reservoir Simulation Conference*.

He, X., Santoso, R., & Hoteit, H. (2020). Application of machine-learning to construct equivalent continuum models from high-resolution discrete-fracture models. *International Petroleum Technology Conference*.

He, X., Zhu, W., Santoso, R., Alsinan, M., Kwak, H., & Hoteit, H. (2021a). CO2 Leakage Rate Forecasting Using Optimized Deep Learning. *SPE Annual Technical Conference and Exhibition*.

He, X., Zhu, W., Santoso, R., Alsinan, M., Kwak, H., & Hoteit, H. (2021b). Fracture Permeability Estimation Under Complex Physics: A Data-Driven Model Using Machine Learning. *SPE Annual Technical Conference and Exhibition*.

Kwak, H., Gao, J., & Harbi, A. (2019). Improving the Permeability Derivation from NMR Data for Reservoir Rocks with Complicated Pore Connectivity. *SPE Middle East Oil and Gas Show and Conference*.

Legland, D., Kiêu, K., & Devaux, M.-F. (2007). Computation of Minkowski measures on 2D and 3D binary images. *Image Analysis & Stereology*, **26**(2), 83–92.

Li, Y., HE, X., AlSinan, M., Ugolkov, E., Kwak, H., & Hoteit, H. (2022). Numerical Study of Surface Roughness Influence on NMR T2 Response. *83rd EAGE Annual Conference & Exhibition*, 2022(1), 1–5.

Li, Y., He, X., Zhu, W., AlSinan, M., Kwak, H., & Hoteit, H. (2022). Digital Rock Reconstruction Using Wasserstein GANs with Gradient Penalty. *International Petroleum Technology Conference*.

Mohnke, O., & Klitzsch, N. (2010). Microscale Simulations of NMR Relaxation in Porous Media Considering Internal Field GradientsAll rights reserved. No part of this periodical may be reproduced or transmitted in any form or by any means, electronic or mechanical, including photocopying, recording, or any information storage and retrieval system, without permission in writing from the publisher. *Vadose Zone Journal*, **9**(4), 846–857.

Mosser, L., Dubrule, O., & Blunt, M. J. (2017). Reconstruction of three-dimensional porous media using generative adversarial neural networks. *Physical Review E*, **96**(4), 043309.

Santoso, R., He, X., Alsinan, M., Kwak, H., & Hoteit, H. (2021). Bayesian long-short term memory for history matching in reservoir simulations. *SPE Reservoir Simulation Conference*.

Santoso, R., He, X., & Hoteit, H. (2019). Application of machine-learning to construct simulation models from high-resolution fractured formation. *Abu Dhabi International Petroleum Exhibition & Conference*.

Tadjer, A., Hong, A., & Bratvold, R. B. (2021). Machine learning based decline curve analysis for short-term oil production forecast. *Energy Exploration & Exploitation*, **39**(5), 1747–1769.

Talabi, O. A. (2008). Pore-scale simulation of NMR response in porous media.

Wang, Y. da, Armstrong, R. T., & Mostaghimi, P. (2020). Boosting resolution and recovering texture of 2D and 3D micro-CT images with deep learning. *Water Resources Research*, **56**(1), e2019WR026052.

Wang, Y., Arns, C. H., Rahman, S. S., & Arns, J.-Y. (2018). Porous structure reconstruction using convolutional neural networks. *Mathematical Geosciences*, **50**(7), 781–799.